Neuron
Article

Thalamocortical Inputs Show Post-Critical-Period Plasticity

Xin Yu,[1,6] Seungsoo Chung,[2,4,6] Der-Yow Chen,[1] Shumin Wang,[1,5] Stephen J. Dodd,[1] Judith R. Walters,[3] John T.R. Isaac,[2,7,*] and Alan P. Koretsky[1,*]
[1]Laboratory of Functional and Molecular Imaging
[2]Developmental Plasticity Section
[3]Neurophysiological Pharmacology Section
National Institute of Neurological Disorders and Stroke, National Institutes of Health, Bethesda, MD 20892, USA
[4]Brain Korea 21 Project for Medical Science, Department of Physiology, Yonsei University College of Medicine, Seoul 120-752, Republic of Korea
[5]Department of Electrical and Computer Engineering, Auburn University, Auburn, AL 36849, USA
[6]These authors contributed equally to this work
[7]Present address: Eli Lilly and Company, Windlesham, Surrey GU20 6PH, UK
*Correspondence: isaacjo@lilly.com (J.T.R.I.), koretskya@ninds.nih.gov (A.P.K.)
DOI 10.1016/j.neuron.2012.04.024

SUMMARY

Experience-dependent plasticity in the adult brain has clinical potential for functional rehabilitation following central and peripheral nerve injuries. Here, plasticity induced by unilateral infraorbital (IO) nerve resection in 4-week-old rats was mapped using MRI and synaptic mechanisms were elucidated by slice electrophysiology. Functional MRI demonstrates a cortical potentiation compared to thalamus 2 weeks after IO nerve resection. Tracing thalamocortical (TC) projections with manganese-enhanced MRI revealed circuit changes in the spared layer 4 (L4) barrel cortex. Brain slice electrophysiology revealed TC input strengthening onto L4 stellate cells due to an increase in postsynaptic strength and the number of functional synapses. This work shows that the TC input is a site for robust plasticity after the end of the previously defined critical period for this input. Thus, TC inputs may represent a major site for adult plasticity in contrast to the consensus that adult plasticity mainly occurs at cortico-cortical connections.

INTRODUCTION

Experience is a potent force that shapes brain circuits and function. Elucidating how sensory experience influences cortical sensory representations has been at the forefront of understanding the mechanisms of experience-driven cortical plasticity (Buonomano and Merzenich, 1998; Fox, 2009; Karmarkar and Dan, 2006; Majewska and Sur, 2006; Ramachandran, 2005). Such plasticity is greatest during postnatal development during certain ''critical periods'' but is also extensively documented in the adult brain including human cortex (Hensch, 2004; Hooks and Chen, 2007; Hummel and Cohen, 2005; Knudsen, 2004). Adult plasticity can be induced in response to deprivation of sensory input, for example due to peripheral nerve injury or amputation (Kaas, 1991; Kaas and Collins, 2003; Wall et al., 2002). The site(s) and mechanism(s) of adult cortical plasticity are not well characterized. The relative contributions of cortical-cortical synaptic changes across the cortical layers or the extent of changes in ascending thalamocortical projections remains unsettled (Cooke and Bear, 2010; Fox et al., 2002; Jones, 2000; Kaas et al., 2008).

Recently, there has been growing interest in using MRI to map plasticity in the adult rodent brain (Dijkhuizen et al., 2001; Pelled et al., 2007b, 2009; van Meer et al., 2010; Yu et al., 2010). Blood-oxygen-level-dependent functional MRI (BOLD-fMRI) techniques have been extensively used in humans and animals to investigate changes in brain function (Cramer et al., 2011). However, the underlying neurovascular coupling mechanism of BOLD-fMRI limits its functional mapping specificity (Logothetis et al., 2001; Uğurbil et al., 2003). Manganese-enhanced MRI (MEMRI) can provide high-resolution MRI for in vivo tracing of neuronal circuits (Bilgen et al., 2006; Canals et al., 2008; Murayama et al., 2006; Pautler et al., 1998; Van der Linden et al., 2002). Manganese (Mn^{2+}) is calcium analog, which can mimic calcium entry into neurons and allow activity-dependent Mn accumulation to make MRI map of activation (Lin and Koretsky, 1997; Yu et al., 2005, 2008). Furthermore, Mn^{2+} crosses synapses and may report synaptic strength (Narita et al., 1990). Indeed, a few studies have attributed changes in MEMRI signal to synaptic plasticity (Pelled et al., 2007a; Van der Linden et al., 2002, 2009; van der Zijden et al., 2008; van Meer et al., 2010; Yu et al., 2007). Recently, it has been shown that MEMRI can track neuronal circuits with laminar specificity, opening up the possibility of identifying sites of plasticity with high resolution (Tucciarone et al., 2009).

In the present study, we use both BOLD-fMRI and MEMRI combined with subsequent brain slice electrophysiology to identify a location and mechanism of plasticity in a model of peripheral deprivation of sensory input from the whiskers in 4- to 6-week-old rats. The cortical representation of the whiskers is in the barrel cortex, which contains clusters of cells termed

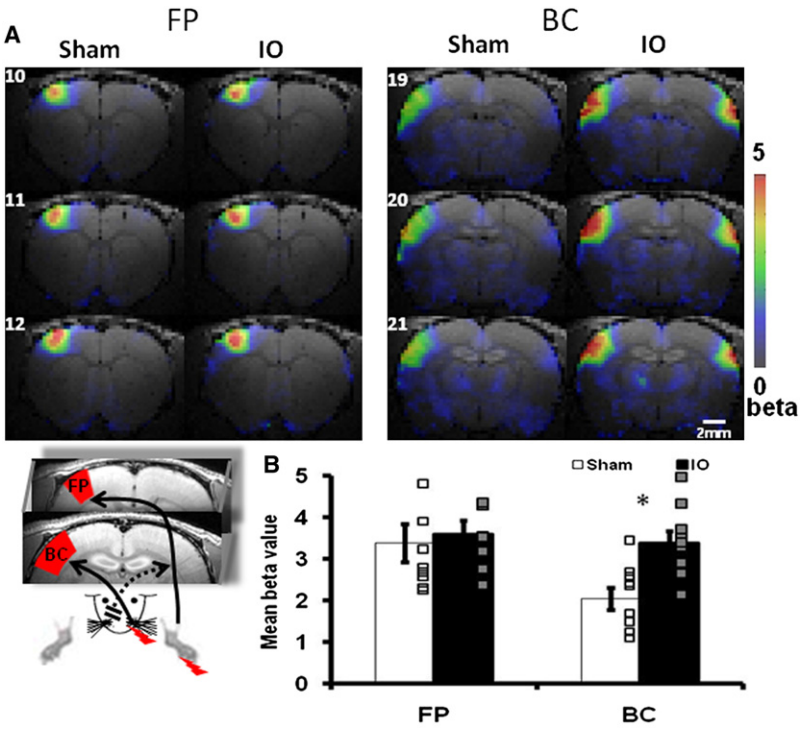

Figure 1. IO Nerve Resection Causes Bilaterally Increased BOLD Responses in the Barrel Cortex

(A) The averaged beta maps of three consecutive coronal slices cover forepaw (FP, 10–12) and barrel cortex (BC, 19–21) S1 areas. The stimulation was delivered to the right forepaw and the spared whisker pad (inset, FP and BC ROIs in red contour defined by atlas).

(B) Quantitative group analysis showed significantly increased BOLD signal in the contralateral BC of the IO rats (BOLD signal changes were defined as mean beta value [Supplemental Note 2]; Sham: n = 9, IO: n = 9; *$p < 0.01$, bar graph shows mean ± SEM).

See also Figure S1.

"barrels" that are the anatomical correlates of the whisker receptive fields (Woolsey and Van der Loos, 1970). Both the development and adult organization of the barrel cortex is highly sensitive to sensory experience (Daw et al., 2007b; Feldman and Brecht, 2005; Fox, 2002; Van der Loos and Woolsey, 1973). For adult barrel cortex, the prevailing view is that plasticity is due to changes in cortico-cortical connections with little or no contribution from thalamocortical or subcortical mechanisms. Rather, thalamocortical and subcortical plasticity is restricted to well-defined "critical periods" early in life.

In the present study, post critical period plasticity of the TC input from the spared whiskers was identified as a prominent mechanism in 6-week-old rats, two weeks after unilateral infraorbital (IO) nerve resection. The TC plasticity was identified using BOLD-fMRI and MEMRI techniques combined with subsequent analysis of the synaptic mechanisms using brain slice electrophysiology. The results provide clear evidence that the TC input to L4 is strengthened even though peripheral nerve resection was performed after the end of the TC critical period. Furthermore, this work shows for the first time the ability for MRI to guide patch clamp electrophysiology to identify the laminar-specific site(s) of modification underlying plasticity in the brain.

RESULTS

BOLD-fMRI Mapping of Plasticity

Six-week-old rats that had undergone unilateral IO nerve resection ("IO rats") or sham surgery ("sham rats") at 4 weeks of age were imaged by MRI. To assess plasticity of circuits activated by the spared input, the BOLD response elicited by electrical stimulation of the intact whisker pad was measured. In addition, the right forepaw was also stimulated in the same rats so that the BOLD response in the forepaw S1 (FP) area could be used as an internal control for the plasticity-induced changes in the barrel cortex (Figure 1, inset). To identify specific regions, we coregistered the MRI with a brain atlas (Figures S1A–S1C, available online; also see Experimental Procedures). Along the whisker-barrel pathway, increased BOLD responses in IO rats compared to sham were detected in the contralateral S1 barrel cortex (Figure 1). There was also an increased BOLD response in ipsilateral S1 barrel cortex. In contrast, the BOLD responses elicited by right forepaw stimulation were not different between the two experimental groups. Thus, unilateral IO nerve resection in four week old rats causes a specific increase in the BOLD response to the activation of the spared input in the barrel cortex.

To determine if there was any change in the relation between thalamic and cortical fMRI response, functional changes in the ventral posteriomedial nucleus (VPM) of thalamus, which receives ascending input from the whiskers, were analyzed (Figure 2, inset). Stimulation of the spared input elicited a BOLD response in the contralateral VPM as expected (Figure S1D). Five increasing stimulus intensities were used and the responses in VPM between IO and sham rats were compared (see Experimental Procedures for details). At all intensities the VPM BOLD response was not different between the two groups; however, in the same animals the S1 barrel cortex BOLD responses were larger in IO rats compared to sham (Figures 2 and S2; Table S1; e.g., at 3.0 mA, the BOLD signal changes of BC in the IO group is increased 50% compared to sham). When the VPM BOLD response was plotted against the S1 BOLD response to produce an input-output plot, there was an increased slope in IO rats compared to sham, showing a 60% cortical potentiation in response to activation of spared input (Figure 3). To confirm the increased neuronal responses in the barrel cortex as shown by BOLD-fMRI, in vivo electrophysiological recordings were performed to analyze whisker pad stimulation-evoked potentials in both L4 barrel cortex and VPM across a range of stimulation intensities (Supplemental Note 1). Consistent with the BOLD-fMRI data, there was no difference in the evoked potentials in VPM between the two groups; however, in

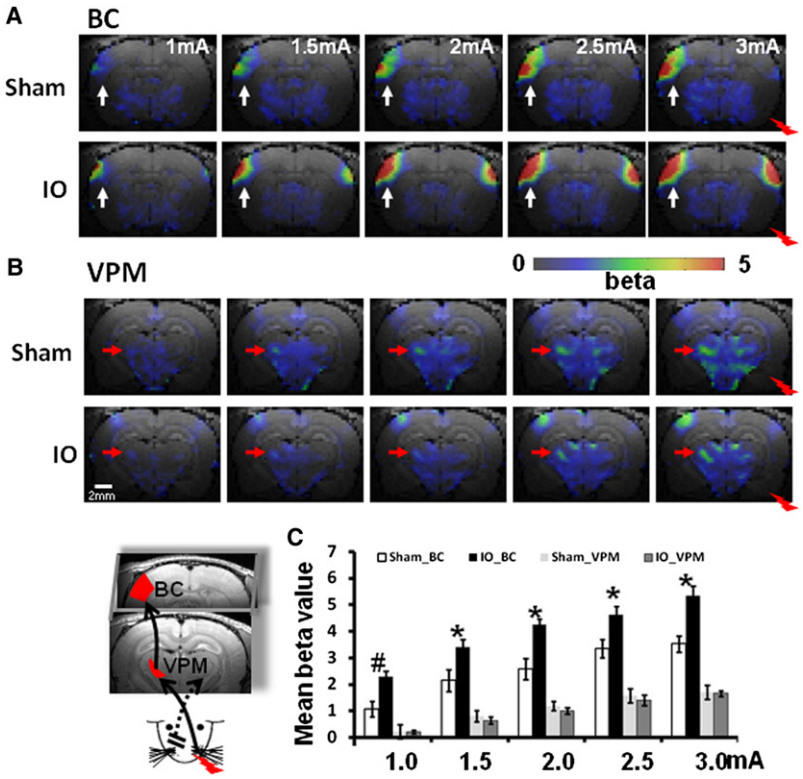

Figure 2. BOLD Responses in BC and VPM Increase Corresponding to the Increased Stimulation Intensities

The schematic drawing of whisker-barrel TC circuit is shown in the inset at the left-bottom corner. The averaged beta maps of barrel cortex (BC) (A, white arrow) and VPM (B, red arrow) at five stimulation intensities from 1 mA to 3 mA.

(C) The averaged mean beta values of BC and VPM ROIs (defined by brain atlas shown in the inset; Sham: n = 8 (3 at 1.0 mA); IO: n = 10 (4 at 1.0 mA); #$p < 0.02$; *$p < 0.01$, bar graph shows mean ± SEM). The averaged fMRI time courses for each ROI were shown in the Figure S2.

See also Figures S2 and S3 and Tables S1 and S2.

the same animals the evoked potentials in L4-barrel cortex were larger in IO rats compared to sham (Table S2; e.g., at 3.0 mA, the evoked potential amplitude in L4-BC in the IO group is increased 36% compared to sham). By measuring the slope of the input-out relationship (L4-BC versus VPM), we observed a significantly steeper slope in IO rats compared to sham, showing a 49% cortical potentiation in response to stimulation of the spared whisker pad (Figure S3). This result demonstrates that the plasticity observed in spared cortex is very likely due to cortical modification and involves TC inputs.

MEMRI Identifies the Layer 4 Barrel Cortex as a Site of Cortical Plasticity

BOLD-fMRI identified S1 contralateral barrel cortex as a prominent site of plasticity in the response to spared input activation. To investigate the mechanisms at this site of plasticity, MEMRI were used to determine if the plasticity could be explained by strengthening of the TC input. Numerous studies provide evidence that changes in Mn^{2+} transport reflects plasticity (Pelled et al., 2007a; Van der Linden et al., 2002, 2009; van der Zijden et al., 2008; van Meer et al., 2010), and laminar resolution tracing with MEMRI has been demonstrated (Tucciarone et al., 2009). Mn^{2+} was injected into dorsal thalamus encompassing VPM (Figure S4) to determine if the spared TC input to barrel cortex is modified by unilateral IO nerve resection. A prominent MEMRI signal was observed in L4 of barrel cortex and the intensity of this signal was greater in IO rats compared to sham (Figure 4). In the same rats, the Mn^{2+}-enhanced signal in L4 of the paw representation was not different between the two groups. In addition, no difference in Mn^{2+} was detected at the injection sites between VPM and ventral posteriomedial nucleus (VPL) in either group (Figure S4). Therefore, the MEMRI data indicate that IO nerve resection may increase TC input strength to L4 specifically in barrel cortex for the spared input.

IO Nerve Resection Causes an Increase in Thalamocortical Input Strength to Layer 4 of the Spared Barrel Cortex

To investigate the underlying mechanism for the increased BOLD-fMRI and MEMRI signals in L4 barrel cortex, thalamocortical brain slices were prepared from 6-week-old rats that had undergone either IO nerve resection or sham surgery at 4 weeks. The thalamocortical brain slice preparation allows TC input to barrel cortex to be selectively activated by extracellular stimulation in VPM and resulting synaptic responses to be monitored with extracellular or patch-clamp recordings (Agmon and Connors, 1991; Crair and Malenka, 1995; Isaac et al., 1997). Extracellular field potential recordings were made to measure TC fEPSPs evoked by electrical stimulation in VPM. TC inputs are glutamatergic, with the fEPSP mediated by AMPARs (Agmon and O'Dowd, 1992; Crair and Malenka, 1995; Kidd and Isaac, 1999; Lu et al., 2001). Consistent with this and previous work (Agmon and Connors, 1992; Crair and Malenka, 1995), the fEPSP was reversibly blocked by 10 μM NBQX, an AMPAR antagonist, or a Ca^{2+}-free extracellular solution (Figure S5). These manipulations did not block the small early downward deflection confirming that this small deflection is a presynaptic fiber volley.

The strength of the TC input to layer 4 (contralateral to the intact whisker-pad) in slices prepared from sham or IO rats was compared by measuring the fEPSP: fiber volley (FV) ratio at different stimulus intensities (Figure 5). This input/output (I/O) relationship was significantly steeper in slices from IO rats compared to sham, demonstrating an increase in TC input strength in the spared input side following IO nerve resection. There was a 47% increase in TC synaptic strength in the IO rats compared to sham. To examine whether intracortical (IC) synapses in L4 barrel cortex are strengthened following IO nerve resection, in a separate set of experiments we measured TC fEPSPs and IC fEPSPs in layer 4 (Figure S6). We confirmed the

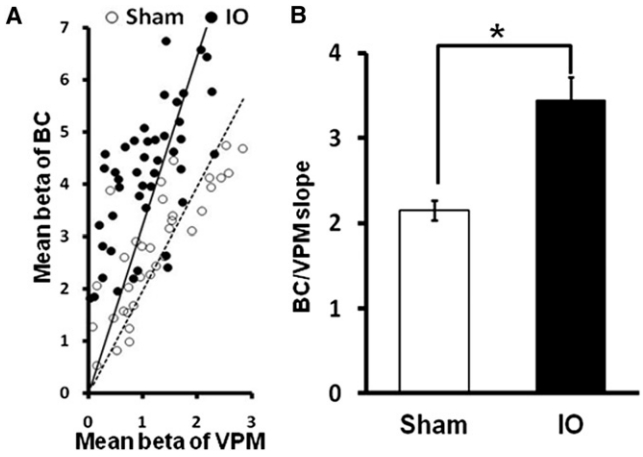

Figure 3. Potentiation of Cortical BOLD Response in BC versus VPM
(A)The scatter plot of the BOLD response in BC and VPM ROIs of individual animals at different stimulation intensity (Sham, open circle; IO, solid circle) with linear fitting (Sham, dotted line; IO, solid line).
(B) The slope of BC/VPM BOLD responses in the IO group compared to the Sham group (Sham: 2.15 ± 0.34, n = 8; IO: 3.45 ± 0.85, n = 10; *p < 0.001, bar graph shows mean ± SEM).
See also Figure S3.

increase in the input/output relationship for TC fEPSPs but found no increase in the input/output relationship for IC fEPSPs in slices from IO rats. Thus, intracortical synaptic strength in layer 4 is not increased in spared barrel cortex in IO rats, indicating strengthening of TC synapses.

No Change in Feedforward Inhibition or Short-Term Plasticity onto L4 Stellate Cells following IO Nerve Resection

The mechanism(s) underlying the increase in the TC fEPSP in the spared barrel cortex were studied with patch-clamp recordings. GABAergic feedforward inhibition in L4 barrel cortex is strongly engaged by TC afferent activity and serves to regulate coincidence detection, truncate the EPSP, and limit spike output in L4 (Chittajallu and Isaac, 2010; Cruikshank et al., 2007; Daw et al., 2007a; Gabernet et al., 2005; Porter et al., 2001). A change in the engagement of feedforward inhibition could contribute to the change of the TC fEPSP observed in the IO rats. Whole-cell voltage-clamp recordings from L4 stellate cells were performed to measure the feedforward inhibition and feedforward excitation onto the same stellate cells using established techniques (Chittajallu and Isaac, 2010; Daw et al., 2007a). The disynaptic feedforward $GABA_A$ receptor-mediated IPSC elicited by VPM stimulation was measured at a holding potential of 0 mV (the reversal potential for the EPSC), and in the same cell in response to the same VPM stimulation the monosynaptic AMPA receptor-mediated TC EPSC was recorded at −70 mV (the $GABA_A$ receptor reversal potential) (Figures 6B and 6C). This ratio of the IPSC:EPSC (“GABA:AMPA ratio”) was unchanged between the IO and sham groups (Figure 6D). Thus, feedforward inhibition as a ratio of feedforward excitation in L4 is unaffected by IO nerve resection indicating that feedforward inhibition scales with the increased feedforward excitatory drive in spared L4 barrel cortex.

The change in the TC input to L4 in IO rats could be due to increases in transmitter release probability (Pr), and/or the number of functional synaptic contacts (n) and/or their quantal size (q). To address the first possibility, short-term plasticity of the TC EPSC in L4 stellate cells was measured. As previously reported, TC inputs to L4 barrel cortex are depressing (e.g., Castro-Alamancos, 2004; Gil et al., 1999; Kidd et al., 2002), and a brief train of VPM stimulation at 50 Hz causes a short-term depression of TC EPSCs (Figure 6E). This short-term plasticity was not different between IO and sham groups (Figure 6F), indicating that presynaptic release probability of glutamate at TC inputs is not altered by IO nerve resection.

IO Nerve Resection Causes an Increase of Quantal Amplitude and Number of Functional Contacts at the Spared TC Input to L4 Stellate Cells

To determine if a postsynaptic modification contributed to the increased TC synaptic strength onto L4 stellate cells in IO rats, the quantal amplitude of AMPAR-mediated TC EPSCs was measured. Substitution of Ca^{2+} with Sr^{2+} in the extracellular medium desynchronizes presynaptic transmitter release producing a barrage of evoked miniature EPSCs after afferent stimulation (Goda and Stevens, 1994). This approach has been used to assay changes in quantal amplitude at the TC input to L4 barrel cortex (Bannister et al., 2005; Gil et al., 1999; Lu et al., 2003). Sr-evoked miniature EPSCs in response to VPM stimulation in L4 stellate cells exhibited an increase in amplitude in the IO rats compared to those in the sham group (Figure 7). In contrast to VPM stimulation-evoked miniature synaptic events, there was no difference in the quantal amplitudes of miniature EPSCs or IPSCs in L4 stellate cells, the majority of which result from transmission at intracortical L4-L4 connections (Lefort et al., 2009; Figure S7). Thus, a postsynaptic increase in quantal amplitude contributes to the increased synaptic strength and is specific to the TC input to L4 in IO rats.

Another possible contribution to the change in TC synaptic strength is an increase in the number of functional synapses onto L4 stellate cells in the IO rats. To address this, a minimal-stimulation protocol was used to measure the postsynaptic response to activation of putative single TC axons e.g., (Chittajallu and Isaac, 2010; Cruikshank et al., 2007; Dobrunz and Stevens, 1997; Gil et al., 1999; Isaac et al., 1997; Raastad et al., 1992; Stevens and Wang, 1995). To elicit putative single TC axon responses, VPM stimulus intensity was reduced until no synaptic responses were observed and then increased in small steps to find an intensity that stably elicited the smallest evoked response (Figures 8A and 8B). This minimal stimulation protocol revealed that in slices from IO rats the minimally evoked EPSC amplitude (excluding failures; “potency”) was greater compared to that in slices from sham animals (Figure 8C). The potency for single fiber activation is dependent on quantal size and number of functional synaptic connections. There was a 37% increase in quantal size measured using Sr-evoked mEPSCs (Figure 7), whereas the potency increase was approximately 65%, demonstrating that IO nerve resection additionally causes an increase in the

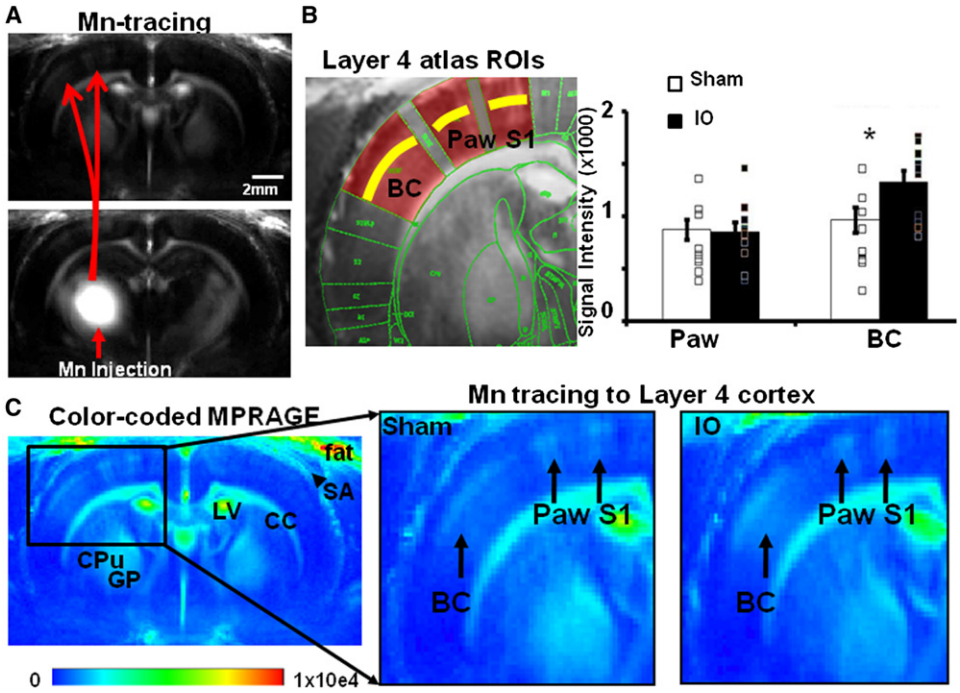

Figure 4. MEMRI Reveals the Strengthening of the TC Input to Layer 4 Barrel Cortex (BC)

(A) Mn tracing from Mn injection site in the dorsal thalamus (VPM+VPL; detail in Figure S3) to the ipsilateral S1 including barrel cortex and paw S1 area.

(B) Left, the atlas overlapped MPRAGE images to define the Layer 4 ROIs in the BC and paw S1 areas. Right, the analysis of MEMRI signal in the L4 of the BC and paw S1 area in IO and Sham groups (Sham: n = 10; IO: n = 9; *p < 0.03, bar graph shows mean ± SEM).

(C) Color-coded MPRAGE images from the sham and IO groups. Left, Mn-enhanced L4 lamina were only located at the same side as the Mn injection. Mn independent signal enhancement was shown in several brain regions in both hemispheres, such as corpus callosum (CC), caudate putamen (CPu), globus pallidus (GP), lateral ventricle (LV), and in the subarachanoid area (SA, arrowhead) and the fat tissue outside the skull. Right, enlarged image to show the Mn-enhanced L4 lamina in both BC and paw S1 areas (black arrows), showing stronger Mn-enhanced signal in the BC L4 of IO rats than that of sham rats. See also Figure S4.

number of functional TC synapses in L4. Taken together, the results show that IO nerve resection causes plasticity of the spared TC input by increasing both quantal amplitude and number of functional synapses.

DISCUSSION

The present study investigates the mechanisms and sites of plasticity induced by loss of whisker sensory input in 6-week-old rats using a combined MRI and slice electrophysiology approach. In contrast to the expectation that plasticity at this age is mediated by modification of cortico-cortical inputs, we found that a prominent plasticity of TC input to L4 underlies the robust increase in spared barrel cortex activation detectable by fMRI. This plasticity was due to a selective increase in quantal amplitude and number of functional synaptic contacts at the TC input to L4 stellate cells while maintaining excitatory/inhibitory balance. This combined MRI and slice electrophysiology approach therefore allows for an analysis of sites and mechanisms of plasticity, which could be broadly applied to many paradigms. The results show that TC inputs can mediate plasticity after the end of the previously defined critical period for this input.

Sensory Deprivation Leads to Thalamocortical Strengthening in IO Rats

IO nerve resection was the sensory manipulation used to induce experience-dependent plasticity in barrel cortex. The IO nerve carries all sensory information from the whiskers, but does not contain motor afferents; therefore, this manipulation results in a complete loss of whisker-dependent sensory input with no loss of motor innervation to the whiskers. The increase in cortical BOLD-fMRI responses after 2 weeks of IO nerve resection in response to electrical stimulation of the spared whisker pad is likely due to increased cortical neuronal activity. Although there are a few examples in which BOLD-fMRI has not been associated with corresponding changes in neuronal activity (Maier et al., 2008; Sirotin and Das, 2009), a proportional increase of BOLD and neuronal signals has been observed in functional mapping studies across a variety of species including rodent, monkey, and human (Heeger et al., 2000; Logothetis et al., 2001; Ogawa et al., 2000; Rees et al., 2000), including for somatosensory cortex (Goloshevsky et al., 2008; Hyder et al., 2002). Indeed, in the present study in vivo electrophysiology directly demonstrates a potentiation of cortical responses in IO rats (Figure S3; Table S1 and S2), which is consistent with a recent study, showing that 2 week denervation of the rat forepaw led to a BOLD-fMRI

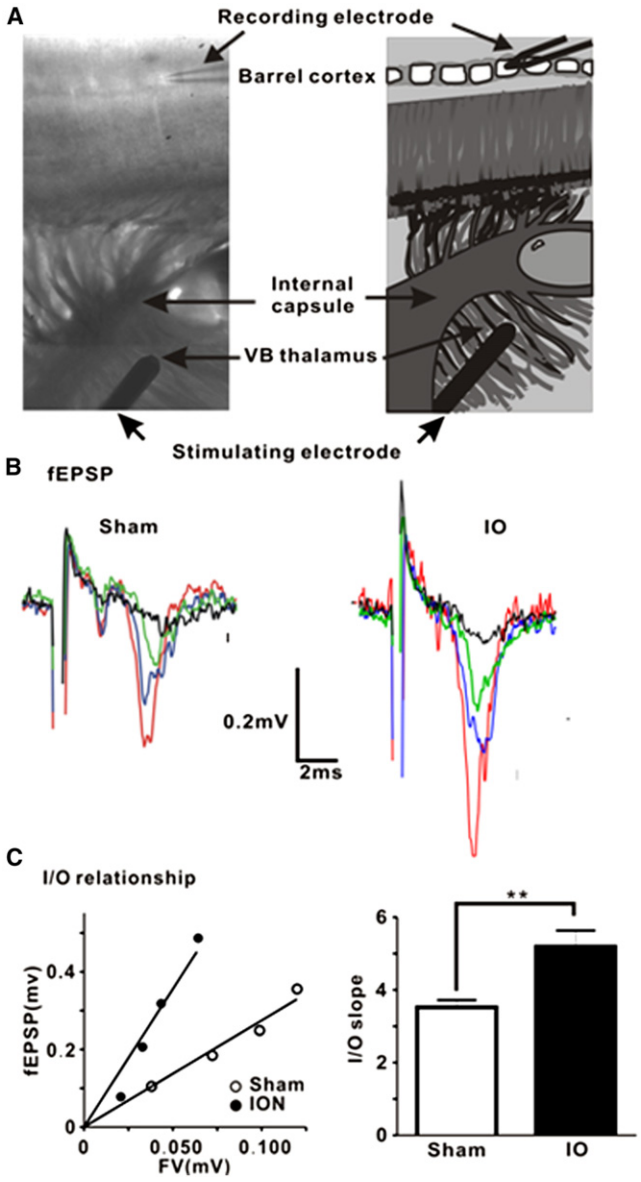

Figure 5. IO Nerve Resection Causes an Increase in TC fEPSPs in Spared Layer 4 Barrel Cortex

(A) Thalamocortical brain slice extracellular recording setup and the corresponding diagram.

(B) Representative superimposed traces of fEPSPs from TC slices from example experiments at four increasing stimulus intensities.

(C) Left panel, scatter plot of the I/O relationship corresponding to the recorded fEPSPs in (B). Sham, $y = 2.87x$, $r^2 = 0.80$, open circles; IO, $y = 6.59x$, $r^2 = 0.82$, filled circles. Right panel, averaged slope of I/O relationship for Sham and IO group (Sham: 3.52 ± 0.20, n = 20; ION: 4.96 ± 0.04, n = 13; **$p < 0.01$, bar graph shows mean ± SEM).

See also Figures S5 and S6.

increase in the spared forepaw S1 that was related to the increases in local field potential (Pelled et al., 2009).

Plasticity at multiple sites could potentially cause the altered BOLD-fMRI response in the barrel cortex of IO rats. The finding of increased activation in the barrel cortex versus changes in VPM activation points strongly to cortical site(s) of plasticity. The MEMRI data further indicate that L4 barrel cortex is a major site of plasticity and the slice electrophysiology shows that the TC input to L4, but not cortico-cortical synapses, are potentiated in spared cortex. In the present work we also found ipsilateral activation of barrel cortex in response to stimulation of the spared input. This is consistent with the previous study showing ipsilateral BOLD-fMRI responses in the deprived forepaw S1 cortex (Pelled et al., 2009). A detailed analysis of the mechanisms for this ipsilateral response will be the subject of a future study.

Numerous reports provide evidence for modification of intracortical synapses for L4 barrel plasticity in adolescent and adult rodents with no contribution from plasticity at TC inputs in a variety of different manipulations (Armstrong-James et al., 1994; Diamond et al., 1993, 1994; Fox, 1992; Fox et al., 2002; Rema et al., 2006; Wallace and Fox, 1999). This is consistent with the critical period for TC plasticity being restricted to the first postnatal week (Brecht, 2007; Diamond et al., 1994; Fox, 1992; Fox et al., 2002). This TC critical period corresponds to a time when silent synapses are present and long-term synaptic plasticity can be induced at TC inputs to L4 (Crair and Malenka, 1995; Daw et al., 2007b; Feldman et al., 1998; Isaac et al., 1997; Kidd and Isaac, 1999). Nevertheless, in contrast to the observations on the slice preparation studies, there is growing evidence to show the potential contribution of changes of TC inputs to adult brain plasticity detected in vivo (Cooke and Bear, 2010; Hogsden and Dringenberg, 2009; Lee and Ebner, 1992). In the present study, the MEMRI and slice electrophysiology data demonstrate that changes in TC inputs to L4 make a major contribution to experience dependent plasticity in the mature brain past the end of the TC critical period. There is evidence from a recent study showing altered TC axonal innervation to L4 barrels of adolescent and adult rats following chronic whisker manipulations (Wimmer et al., 2010). Other studies show that the dendritic arborization pattern and the density of excitatory/inhibitory synapses in L4 barrels are sensitive to whisker experience in adult animals (Knott et al., 2002; Tailby et al., 2005). Such anatomical changes are consistent with our MEMRI tracing data. Indeed, the MEMRI signal may reflect a contribution from Mn^{2+} accumulated in dendritic arbors of L4 neurons because the transsynaptic transport becomes more efficient due to synaptic strengthening.

Mechanisms of Experience-Dependent Plasticity in Adult Barrel Cortex

Our data show that strengthening of the TC input to L4 stellate cells in spared barrel cortex is a prominent mechanism for plasticity in the mature brain after peripheral nerve injury. TC inputs strongly engage feedforward inhibitory interneurons in L4 barrel cortex (Chittajallu and Isaac, 2010; Cruikshank et al., 2007; Daw et al., 2007a; Gabernet et al., 2005; Porter et al., 2001; Sun et al., 2006), and notably the ratio of feedforward inhibition and excitation in L4 was unaffected in IO rats. This demonstrates that inhibition was similarly potentiated with the increased excitation in these animals. This parallel enhancement of feedforward inhibition could be due to an increase in TC input strength onto

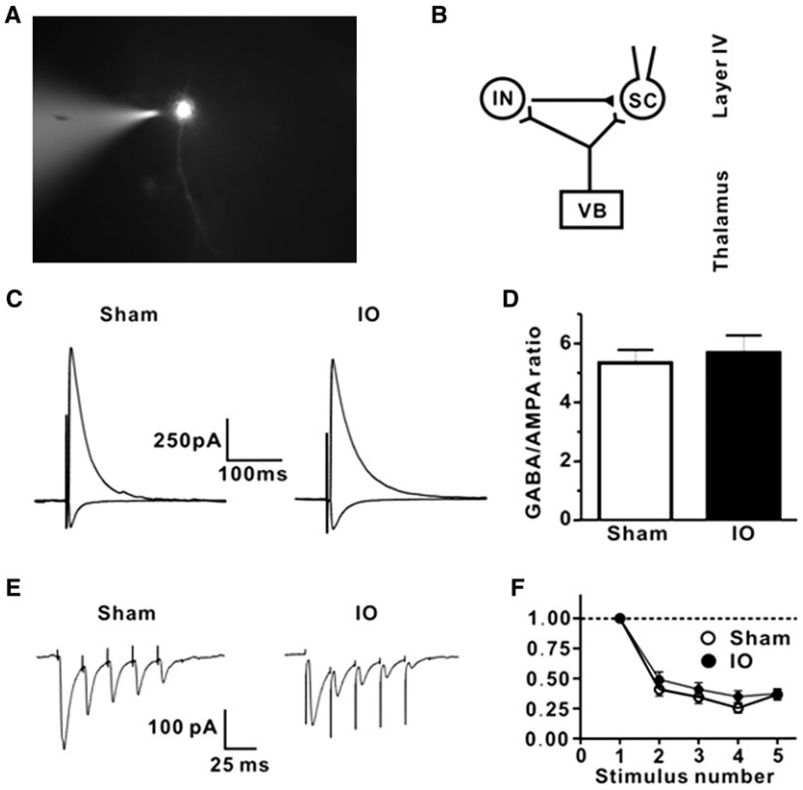

Figure 6. IO Nerve Resection Has No Effect on Feedforward Inhibition or Short-Term Plasticity at TC Inputs to Layer 4

(A) Patch-clamp recording on a L4 stellate cell.

(B) The diagram of TC feedforward monosynaptic excitatory and feedforward disynaptic inhibition pathway.

(C) Representative traces of TC $GABA_A$ receptor-mediated IPSC (average of 5 sweeps; outward current) at 0 mV holding potential and TC EPSC (average of 5 sweeps; inward current) at −70 mV in L4 stellate cells from Sham and IO nerve resection groups.

(D) Analysis of $GABA_A$ receptor-mediated IPSC amplitude to AMPAR-mediated EPSC ratio for all cells (Sham: 5.34 ± 0.31, n = 10, open bars; IO: 5.82 ± 0.46, n = 9, filled bars, bar graph shows mean ± SEM).

(E) Representative traces of train-stimulation evoked EPSCs (50Hz; average of 10 trials) for two groups.

(F) Analysis of EPSC amplitude during trains (normalize to first EPSC in train) for both groups (Sham n = 7, IO n = 9, the plot shows mean ± SEM.).

feedforward interneurons, and/or an increase in their excitability and/or an increase in their connectivity to stellate cells. In other studies, it has been shown that during development the excitability of feedforward interneurons, the strength of TC inputs onto feedforward interneurons and the strength of inhibitory synaptic transmission onto stellate cells in L4 barrel cortex can all be regulated by whisker-driven activity (Chittajallu and Isaac, 2010; Jiao et al., 2006; Sun et al., 2009). Furthermore, the most prominent effect of whisker activity on synaptic anatomy is an increase in GABAergic synapses (Knott et al., 2002). Thus multiple mechanisms could contribute to the scaling of inhibition with excitation in L4 barrel cortex.

The spared TC input exhibits increased quantal amplitude and an increased number of functional synapses. This is suggestive of an LTP mechanism underlying the strengthening of the spared input. There is considerable evidence that long-term synaptic plasticity mechanisms underlie experience-dependent plasticity in primary sensory cortical areas (Feldman, 2009; Malenka and Bear, 2004). However, previous studies have demonstrated that both LTP and LTD at TC inputs in L4 barrel cortex declines during the first postnatal week and is absent by the second postnatal week (Crair and Malenka, 1995; Daw et al., 2007b; Feldman et al., 1998; Isaac et al., 1997). Thus, our results suggest that the two week loss of sensory input to the contralateral barrel cortex in 4- to 6-week-old rats reactivates LTP-like plasticity at TC inputs in spared barrel cortex.

It is not clear whether the increased TC input underlies the full BOLD-fMRI increase detected in the cortex of IO rats. Although our findings on a lack of change in the IC fEPSP and in spontaneous EPSCs and IPSCs suggest no local change in intracortical synaptic strength in L4, it is probable that other mechanisms outside L4 could act in addition to TC input strengthening to contribute to the increased BOLD signal observed. In addition, IO nerve resection may modify subcortical and long range cortical connections to mediate an increase in excitability of the L4 network in response to stimulation of input to spared cortex. Such mechanisms would not be readily detectible in slice preparations, and would be a topic for future studies.

In conclusion, our data demonstrate that TC inputs to L4 can be a site of plasticity after the end of the critical period. Moreover, the use of the combined MRI and electrophysiology approach provides a powerful method for whole-brain mapping of plasticity mechanisms that would be readily applicable to a number of lesion, behavioral, and pharmacological paradigms.

EXPERIMENTAL PROCEDURES

Infraorbital Denervation

All animal work was performed according to the guidelines of the Animal Care and Use Committee and the Animal Health and Care Resection of the National Institute of Neurological Disorders and Stroke, National Institutes of Health (Bethesda, MD, USA). Four-week-old Sprague-Dawley rats were anesthetized with isoflurane. The infraorbital denervation procedure was described previously (Dietrich et al., 1985). Briefly, the infraorbital branch of the trigeminal nerve was first exposed as it emerges from the infraorbital foramen in a broad band of fibers fanning out in all directions to the skin of the snout and to the vibrissal roots. The infraorbital fiber bundles were stretched from the infraorbital foramen and then tightly ligated just distal to the infraorbital foramen to prevent regeneration. Up to 2–3 mm distal to the ligature was cauterized toward the vibrissal roots. For those undergoing a sham procedure, incisions were made and the nerve exposed, but nerve bundle ligation and cauterization was not performed. Rats were allowed to recover for 14–18 days before MRI imaging and electrophysiological recordings. The proximal stump of the cauterized nerve was examined following MRI, and no signs of regrowth toward the whisker pad and snout area from the infraorbital foramen were observed. There were a total 58 IO and 52 sham rats. Among all of these

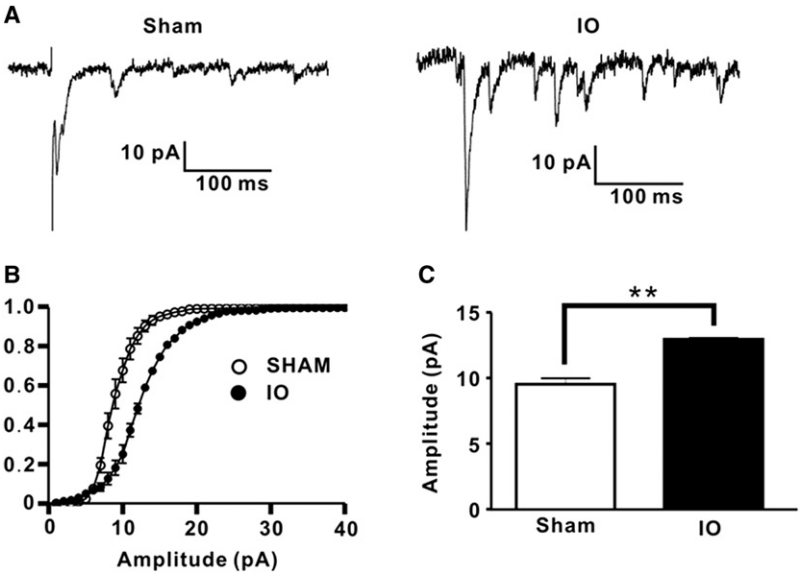

Figure 7. IO Nerve Resection Causes an Increase in Quantal Amplitude at TC Inputs to Layer 4 Stellate Cells

(A) Representative traces of Sr-evoked miniature EPSCs for both groups.

(B) Averaged cumulative probability plot of Sr-evoked miniature EPSCs for all cells for both groups (Sham: n = 7, open circles; IO: n = 5, filled circles; Kolmogrov-Smirnov test, $p < 0.01$, the plot show mean ± SEM.).

(C) Mean amplitude of Sr^{2+} -evoked miniature EPSCs for both groups (Sham: 9.35 ± 0.46, n = 7; IO: 12.70 ± 0.29, n = 5; **$p < 0.01$, bar graph shows mean ± SEM).

See also Figure S7.

rats, 28 IO and 27 sham rats were used for MRI imaging, and 30 IO and 25 sham rats were used for electrophysiological recordings.

Animal Preparation for Functional MRI

MRI was performed as previously described (Yu et al., 2010). Rats were initially anesthetized with isoflurane. Each rat was orally intubated and placed on a mechanical ventilator. Plastic catheters were inserted into the right femoral artery and vein to allow monitoring of arterial blood gases and administration of drugs. After surgery, all rats were given i.v. bolus of α-chloralose (80 mg/kg) and isoflurane was discontinued. Anesthesia was maintained with a constant infusion of α-chloralose (26.5 mg/kg/h) in combination with pancuronium bromide (4 mg/kg/hr) to reduce motion artifacts. A heated water pad maintained rectal temperature at ~37.5°C. Each rat was secured in a head holder with a bite bar to prevent head motion. End-tidal CO_2, rectal temperature, tidal pressure of ventilation, heart rate, and arterial blood pressure were continuously monitored during the experiment. Arterial blood gas levels were checked periodically, and corrections were made by adjusting respiratory volume or administering sodium bicarbonate to maintain normal levels.

Electrical stimulation of the whisker pad and forepaw was described in our previous study (Yu et al., 2010; Berwick et al., 2004). For the forepaw stimulation, two needle electrodes were inserted between digits 1, 2 and 3, 4. For whisker pad stimulation, an electrode pad with five pins (one cathode in the center of a 5 × 5 mm square with four anodes at each corner) was designed. To reduce the cross-subject variation, the center pin was positioned at the third whisker of the caudal side of row C for each rat. An isolated stimulator (WPI, FL) supplied 330 μs pulses repeated at 3 Hz to the whisker pad and forepaw simultaneously upon demand at varying amount. The electrical current was set from 1.0 to 3.0 mA with 0.5 mA increments to the whisker pad. It is noteworthy that electrical stimulation at 2.5–3.0 mA led to the subcortical BOLD-fMRI responses in the ipsilateral thalamic area and habenular nuclei, which could be related to pain processing at the high stimulation intensities (Hikosaka, 2010).

Mn-Tracing Preparation

A detailed procedure was described previously (Tucciarone et al., 2009). For thalamic injections, rats received 250 nl of 50 mM $MnCl_2$ solution (0.9% saline) into the left hemisphere (Bregma −3.0, lateral − 3.0, and ventral 5.7 mm), contralateral to the intact whisker pad of IO rats. The stereotactic coordinates were determined according to the Paxinos and Watson (2007) atlas. Animals were anesthetized by isoflurane. A small bur hole was drilled after exposing the skull. A homemade glass injection needle was placed at the proper coordinates in the stereotactic frame. Injections were performed slowly over 5–6 min using a microinjector (Narishige, Tokyo), and the needle was slowly removed after being kept into the injection site for 10 min. MRI was performed right after stereotactic injections to make sure $MnCl_2$ delivered to the proper site and at 4 to 6 hr post injection to analyze Mn in the cortical lamina (Tucciarone et al., 2009). For MRI scans, rats were anaesthetized with 1%–2% isoflurane using a nose cone and rectal temperature was maintained at 37°C ± 1°C by a heated water bath. After surgery and in between scans, the rats were allowed to recover and were free to roam within their cages. No abnormalities were observed after injection in all rats.

MRI Image Acquisition

All images were acquired with an 11.7 T/31 cm horizontal bore magnet (Magnex, Abingdon, UK), interfaced to an AVANCE III console (Bruker, Germany), and equipped with a 12 cm gradient set, capable of providing 100 G/cm with a rise time of 150 μs (Resonance Research, MA). A custom-built 9 cm diameter quadrature transmitter coil was attached to the gradient. A 1 cm diameter surface receive coil with transmitting/receiving decoupling device was used during imaging acquisition. The fMRI imaging setup included shimming, adjustments to echo spacing and symmetry, and B_0 compensation. A 3D gradient-echo, EPI sequence with a 64 × 64 × 32 matrix was run with the following parameters: effective echo time (TE) 16 ms, repetition time (TR) 1.5 s (effective TR 46.875 ms), bandwidth 170 kHz, flip angle 12°, FOV 1.92 × 1.92 × 0.96 cm. A two-block design stimulation paradigm was applied in this study. For the simultaneous forepaw and whisker pad stimulation experiment, the paradigm consisted of 320 dummy scans to reach steady state, followed by 20 scans prestimulation, 20 scans during electrical stimulation, and 20 scans post-stimulation, which was repeated 3 times (140 scans were acquired overall). Six to eight multiple trials were acquired for each rat. For whisker-pad stimulation at different intensities (1.0–3.0 mA), the paradigm consisted of 320 dummy scans to reach steady state, followed by 20 scans prestimulation, 10 scans during electrical stimulation, and 20 scans post-stimulation, which was repeated 3 times (110 scans were acquired overall). Three to five multiple trials were repeated in a random order at different stimulation intensities with a total of 15–20 trials acquired for each rat. For the Mn-tracing study, a magnetization prepared rapid gradient echo (MP-RAGE) sequence (Mugler and Brookeman, 1990) was used. Sixteen coronal slices with FOV = 1.92 × 1.44 cm, matrix 192 × 144, thickness = 0.5 mm (TR = 4000 ms, Echo TR/TE = 15/5 ms, TI = 1000 ms, number of segments = 4, averages = 10) were used to cover the area of interest at 100 μm in-plane resolution with total imaging time 40 min. To measure intensity in the thalamus across animals, a T1-map was acquired using a rapid acquisition with refocused echoes (RARE) sequence with a similar image orientation to the MP-RAGE sequence (TE = 9.6 ms, Multi-TR = 0.5 s, 1 s, 1.9 s, 3.2 s, and 10 s, Rare factor = 2). For the purpose of cross-subject registration, T1-weigted anatomical images were also acquired in the same orientation as that of the 3D EPI and MPRAGE images with the following parameters: TR = 500 ms, TE = 4 ms, flip angle 45°, in-plane resolution 100 μm.

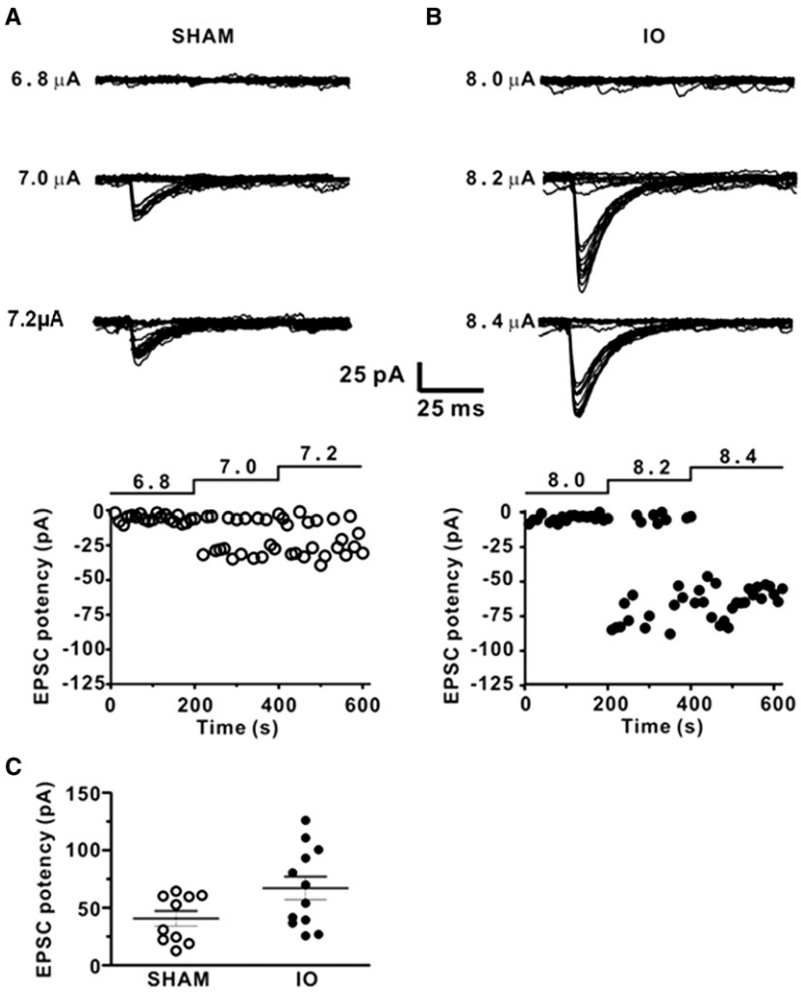

Figure 8. IO Nerve Resection Causes an Increase in Minimal Stimulation-Evoked EPSCs in L4 Stellate Cells

(A) Top superimposed individual traces (20 traces for each stimulus intensity) of EPSCs evoked by minimal stimulation at different intensities (indicated left) for an experiment from the Sham group. Bottom, amplitude of EPSCs plotted versus time with stimulus intensity indicated.

(B) Same as A for IO nerve resection group.

(C) Analysis of TC input potency (mean amplitude of successes ± SEM) for IO and Sham groups (Sham: −40.7 ± 6.5 pA, n = 10; IO: −67.1 ± 10.0 pA, n = 12; $p < 0.05$).

Electrophysiology

Thalamocortical (TC) slices (450 microns) were prepared from adult Sprague-Dawley Rats (6−7 weeks) with some modifications of the method described previously (Agmon and Connors, 1991; Isaac et al., 1997) Briefly, after rats were anesthetized with isoflurane, the brain was rapidly cooled via transcardiac perfusion with ice-cold sucrose- artificial cerebrospinal fluid (CSF). The brain was removed and placed in ice-cold sucrose-artificial CSF. Paracoronal slices were prepared at an angle of 50° relative to the midline on a ramp at an angle of 10°. Then, slices were incubated in artificial CSF at 35°C for 30 min to recover. Slices were then incubated in artificial CSF at room temperature (23°C −25°C) for 1–4 hr before being placed in the recording chamber for experiments. The standard artificial CSF contained (mM) 119 NaCl, 2.5 KCl, 2.5 $CaCl_2$, 1.3 $MgSO_4$, 1.0 NaH_2PO_4, 26.2 NaH_2CO_3, 11 glucose, 1 Na pyruvate, 0.4 Na ascorbate saturated with 95% O_2/5% CO_2. Sucrose-artificial CSF contained (mM) 198 sucrose, 2.5 KCl, 1 NaH_2PO_4, 26.2 $NaHCO_3$, 11 glucose, 1 Na pyruvate, 0.4 Na ascorbate saturated with 95% O_2/5% CO_2. All experiments were conducted at 27°C–29°C.

For electrophysiological experiments, electrodes with 3–6 MΩ pipette resistance were used and stimuli were applied to the VPM using a concentric bipolar electrode (FHC, Bowdoin, ME). The somatosensory cortex was identified by the presence of barrels under low-power magnification and differential interference contrast (DIC) optics and by the ability to evoke short and constant latency fEPSPs by VPM stimulation (Agmon and Connors, 1991). Whole-cell voltage-clamp recordings were made from spiny stellate neurons in layer IV of the somatosensory cortex using infrared illumination and differential interference contrast (DIC) optics. The whole-cell recording solution was as follows (mM): 135 Cs methanesulfonate, 8 NaCl, 10 HEPES, 0.5 EGTA, 4 Mg-ATP, 0.3 Na-GTP and 5 QX-315 Cl (pH 7.25 with CsOH, 285 mOsm). Cells were held at −70 mV during recordings unless otherwise indicated. Recordings were made using a multiclamp 700B (Molecular Devices, Sunnyvale, CA) digitized at 10 KHz and filtered at 2 KHz. Input resistance and series resistance were monitored continuously during recordings, as previously described (Isaac et al., 1995). EPSCs were accepted as monosynaptic if they exhibited a short and constant latency that did not change with increasing stimulus intensity. TC EPSC and EPSPs were evoked at a frequency of 0.1 Hz using a bipolar stimulating electrode placed in the VPM.

To examine disynaptic feedforward inhibition onto stellate cells, we measured IPSC:EPSC ("GABA:AMPA") ratio. The intensity of the stimulus (typically 10–40 V) was adjusted to produce an EPSC of 150–200 pA in amplitude in the stellate cell. The peak amplitude of the $GABA_A$ receptor-mediated IPSC was measured at 0 mV and the peak amplitude of the AMPA receptor-mediated EPSC was measured at −70 mV as previously reported (Chittajallu and Isaac, 2010; Daw et al., 2007a). For experiments on short-term plasticity, the responses to a brief train stimulus (50 Hz) were obtained by averaging 10 trials. For estimation of peak amplitude of each EPSC during a train stimulus, postsynaptic summation was removed, as previously described (Kidd et al., 2002).

To measure evoked miniature EPSCs, stable whole-cell voltage-clamp recordings were performed with artificial CSF in which 4 mM Sr^{2+} was substituted for 4 mM Ca^{2+}. Quantal events were detected and collected within a 200 ms window beginning 100 ms after VPM stimulation using a sliding template algorithm. Miniature EPSCs/IPSCs were also measured (detail experimental procedure in Supplemental Note 1). For the minimal-stimulation protocol, thalamic stimulation intensity was adjusted until the lowest intensity that elicited a mixture of responses and failures was detected. Failure rate was calculated as number of failures/total number of trials. Potency was calculated as the mean EPSC peak amplitude excluding failures (Chittajallu and Isaac, 2010; Isaac et al., 1997; Stevens and Wang, 1995). The criteria for single-axon stimulation were (1) all or none synaptic events, (2) little or no change in the mean amplitude of the EPSC evoked by small increases in stimulus intensity, as previously reported (Chittajallu and Isaac, 2010; Gil et al., 1999). Data was collected for 20 trials at 0.1 Hz.

Imaging Processing and Statistical Analysis

MRI data analysis was performed using Analysis of Functional NeuroImages software (AFNI) (NIH, Bethesda) and C++. Similar to the previously reported imaging processing procedure (Yu et al., 2010), a detailed description is included in Supplemental Note 2. The beta value of each voxel was derived from a linear regression analysis to estimate the amplitude of

BOLD response (Cox, 1996), which is briefly described in the following equation:

$$Y_i = X_i\beta_i + \epsilon_i, \quad i = 1, \ldots, n,$$

(Y_i are the measurements, X_i are the known regressors or predictor variables, β_i are the unknown parameters to be estimated for each voxel, ϵ_i are random errors). The beta value (0–5) estimates the amplitude of the BOLD response in the beta maps as shown in the color bar (Figures 1 and 2). To provide a brain-atlas-based region of interest in the cortex and thalamus of the rat brain, MRI images were registered to the brain atlas using C++ and Matlab programming (Supplemental Note 3). A diagram of the image processing is shown in Figure S1.

Statistics and Graphical Representation

All summary data were presented as mean ± SEM. Statistical analyses were carried out using two-tailed, unpaired t test or the Kolmogorov-Smirnov test as appropriate.

SUPPLEMENTAL INFORMATION

Supplemental Information includes seven figures, two tables, and Supplemental Experimental Procedures and can be found with this article online at doi:10.1016/j.neuron.2012.04.024.

ACKNOWLEDGMENTS

This research was supported by the Intramural Research Program of the NIH, NINDS. We thank Dr. Afonso Silva for his support to provide the in vivo recording environment and the help from Mr. Colin Gerber and Ms. Marian Wahba. We thank Ms. Kathryn Sharer, Ms. Nadia Bouraoud, and Ms. Lisa Zhang for their technical support.

Accepted: April 27, 2012
Published: May 23, 2012

REFERENCES

Agmon, A., and Connors, B.W. (1991). Thalamocortical responses of mouse somatosensory (barrel) cortex in vitro. Neuroscience *41*, 365–379.

Agmon, A., and Connors, B.W. (1992). Correlation between intrinsic firing patterns and thalamocortical synaptic responses of neurons in mouse barrel cortex. J. Neurosci. *12*, 319–329.

Agmon, A., and O'Dowd, D.K. (1992). NMDA receptor-mediated currents are prominent in the thalamocortical synaptic response before maturation of inhibition. J. Neurophysiol. *68*, 345–349.

Armstrong-James, M., Diamond, M.E., and Ebner, F.F. (1994). An innocuous bias in whisker use in adult rats modifies receptive fields of barrel cortex neurons. J. Neurosci. *14*, 6978–6991.

Bannister, N.J., Benke, T.A., Mellor, J., Scott, H., Gürdal, E., Crabtree, J.W., and Isaac, J.T. (2005). Developmental changes in AMPA and kainate receptor-mediated quantal transmission at thalamocortical synapses in the barrel cortex. J. Neurosci. *25*, 5259–5271.

Berwick, J., Redgrave, P., Jones, M., Hewson-Stoate, N., Martindale, J., Johnston, D., and Mayhew, J.E. (2004). Integration of neural responses originating from different regions of the cortical somatosensory map. Brain Res. *1030*, 284–293.

Bilgen, M., Peng, W., Al-Hafez, B., Dancause, N., He, Y.Y., and Cheney, P.D. (2006). Electrical stimulation of cortex improves corticospinal tract tracing in rat spinal cord using manganese-enhanced MRI. J. Neurosci. Methods *156*, 17–22.

Brecht, M. (2007). Barrel cortex and whisker-mediated behaviors. Curr. Opin. Neurobiol. *17*, 408–416.

Buonomano, D.V., and Merzenich, M.M. (1998). Cortical plasticity: from synapses to maps. Annu. Rev. Neurosci. *21*, 149–186.

Canals, S., Beyerlein, M., Keller, A.L., Murayama, Y., and Logothetis, N.K. (2008). Magnetic resonance imaging of cortical connectivity in vivo. Neuroimage *40*, 458–472.

Castro-Alamancos, M.A. (2004). Dynamics of sensory thalamocortical synaptic networks during information processing states. Prog. Neurobiol. *74*, 213–247.

Chittajallu, R., and Isaac, J.T. (2010). Emergence of cortical inhibition by coordinated sensory-driven plasticity at distinct synaptic loci. Nat. Neurosci. *13*, 1240–1248.

Cooke, S.F., and Bear, M.F. (2010). Visual experience induces long-term potentiation in the primary visual cortex. J. Neurosci. *30*, 16304–16313.

Cox, R.W. (1996). AFNI: software for analysis and visualization of functional magnetic resonance neuroimages. Comput. Biomed. Res. *29*, 162–173.

Crair, M.C., and Malenka, R.C. (1995). A critical period for long-term potentiation at thalamocortical synapses. Nature *375*, 325–328.

Cramer, S.C., Sur, M., Dobkin, B.H., O'Brien, C., Sanger, T.D., Trojanowski, J.Q., Rumsey, J.M., Hicks, R., Cameron, J., Chen, D., et al. (2011). Harnessing neuroplasticity for clinical applications. Brain *134*, 1591–1609.

Cruikshank, S.J., Lewis, T.J., and Connors, B.W. (2007). Synaptic basis for intense thalamocortical activation of feedforward inhibitory cells in neocortex. Nat. Neurosci. *10*, 462–468.

Daw, M.I., Ashby, M.C., and Isaac, J.T. (2007a). Coordinated developmental recruitment of latent fast spiking interneurons in layer IV barrel cortex. Nat. Neurosci. *10*, 453–461.

Daw, M.I., Scott, H.L., and Isaac, J.T. (2007b). Developmental synaptic plasticity at the thalamocortical input to barrel cortex: mechanisms and roles. Mol. Cell. Neurosci. *34*, 493–502.

Diamond, M.E., Armstrong-James, M., and Ebner, F.F. (1993). Experience-dependent plasticity in adult rat barrel cortex. Proc. Natl. Acad. Sci. USA *90*, 2082–2086.

Diamond, M.E., Huang, W., and Ebner, F.F. (1994). Laminar comparison of somatosensory cortical plasticity. Science *265*, 1885–1888.

Dietrich, W.D., Ginsberg, M.D., Busto, R., and Smith, D.W. (1985). Metabolic alterations in rat somatosensory cortex following unilateral vibrissal removal. J. Neurosci. *5*, 874–880.

Dijkhuizen, R.M., Ren, J.M., Mandeville, J.B., Wu, O.N., Ozdag, F.M., Moskowitz, M.A., Rosen, B.R., and Finklestein, S.P. (2001). Functional magnetic resonance imaging of reorganization in rat brain after stroke. Proc. Natl. Acad. Sci. USA *98*, 12766–12771.

Dobrunz, L.E., and Stevens, C.F. (1997). Heterogeneity of release probability, facilitation, and depletion at central synapses. Neuron *18*, 995–1008.

Feldman, D.E. (2009). Synaptic mechanisms for plasticity in neocortex. Annu. Rev. Neurosci. *32*, 33–55.

Feldman, D.E., and Brecht, M. (2005). Map plasticity in somatosensory cortex. Science *310*, 810–815.

Feldman, D.E., Nicoll, R.A., Malenka, R.C., and Isaac, J.T. (1998). Long-term depression at thalamocortical synapses in developing rat somatosensory cortex. Neuron *21*, 347–357.

Fox, K. (1992). A critical period for experience-dependent synaptic plasticity in rat barrel cortex. J. Neurosci. *12*, 1826–1838.

Fox, K. (2002). Anatomical pathways and molecular mechanisms for plasticity in the barrel cortex. Neuroscience *111*, 799–814.

Fox, K. (2009). Experience-dependent plasticity mechanisms for neural rehabilitation in somatosensory cortex. Philos. Trans. R. Soc. Lond. B Biol. Sci. *364*, 369–381.

Fox, K., Wallace, H., and Glazewski, S. (2002). Is there a thalamic component to experience-dependent cortical plasticity? Philos. Trans. R. Soc. Lond. B Biol. Sci. *357*, 1709–1715.

Gabernet, L., Jadhav, S.P., Feldman, D.E., Carandini, M., and Scanziani, M. (2005). Somatosensory integration controlled by dynamic thalamocortical feed-forward inhibition. Neuron *48*, 315–327.

Gil, Z., Connors, B.W., and Amitai, Y. (1999). Efficacy of thalamocortical and intracortical synaptic connections: quanta, innervation, and reliability. Neuron *23*, 385–397.

Goda, Y., and Stevens, C.F. (1994). Two components of transmitter release at a central synapse. Proc. Natl. Acad. Sci. USA *91*, 12942–12946.

Goloshevsky, A.G., Silva, A.C., Dodd, S.J., and Koretsky, A.P. (2008). BOLD fMRI and somatosensory evoked potentials are well correlated over a broad range of frequency content of somatosensory stimulation of the rat forepaw. Brain Res. *1195*, 67–76.

Heeger, D.J., Huk, A.C., Geisler, W.S., and Albrecht, D.G. (2000). Spikes versus BOLD: what does neuroimaging tell us about neuronal activity? Nat. Neurosci. *3*, 631–633.

Hensch, T.K. (2004). Critical period regulation. Annu. Rev. Neurosci. *27*, 549–579.

Hikosaka, O. (2010). The habenula: from stress evasion to value-based decision-making. Nat. Rev. Neurosci. *11*, 503–513.

Hogsden, J.L., and Dringenberg, H.C. (2009). Decline of long-term potentiation (LTP) in the rat auditory cortex in vivo during postnatal life: involvement of NR2B subunits. Brain Res. *1283*, 25–33.

Hooks, B.M., and Chen, C. (2007). Critical periods in the visual system: changing views for a model of experience-dependent plasticity. Neuron *56*, 312–326.

Hummel, F.C., and Cohen, L.G. (2005). Drivers of brain plasticity. Curr. Opin. Neurol. *18*, 667–674.

Hyder, F., Rothman, D.L., and Shulman, R.G. (2002). Total neuroenergetics support localized brain activity: implications for the interpretation of fMRI. Proc. Natl. Acad. Sci. USA *99*, 10771–10776.

Isaac, J.T., Nicoll, R.A., and Malenka, R.C. (1995). Evidence for silent synapses: implications for the expression of LTP. Neuron *15*, 427–434.

Isaac, J.T., Crair, M.C., Nicoll, R.A., and Malenka, R.C. (1997). Silent synapses during development of thalamocortical inputs. Neuron *18*, 269–280.

Jiao, Y., Zhang, C., Yanagawa, Y., and Sun, Q.Q. (2006). Major effects of sensory experiences on the neocortical inhibitory circuits. J. Neurosci. *26*, 8691–8701.

Jones, E.G. (2000). Cortical and subcortical contributions to activity-dependent plasticity in primate somatosensory cortex. Annu. Rev. Neurosci. *23*, 1–37.

Kaas, J.H. (1991). Plasticity of sensory and motor maps in adult mammals. Annu. Rev. Neurosci. *14*, 137–167.

Kaas, J.H., and Collins, C.E. (2003). Anatomic and functional reorganization of somatosensory cortex in mature primates after peripheral nerve and spinal cord injury. Adv. Neurol. *93*, 87–95.

Kaas, J.H., Qi, H.X., Burish, M.J., Gharbawie, O.A., Onifer, S.M., and Massey, J.M. (2008). Cortical and subcortical plasticity in the brains of humans, primates, and rats after damage to sensory afferents in the dorsal columns of the spinal cord. Exp. Neurol. *209*, 407–416.

Karmarkar, U.R., and Dan, Y. (2006). Experience-dependent plasticity in adult visual cortex. Neuron *52*, 577–585.

Kidd, F.L., and Isaac, J.T. (1999). Developmental and activity-dependent regulation of kainate receptors at thalamocortical synapses. Nature *400*, 569–573.

Kidd, F.L., Coumis, U., Collingridge, G.L., Crabtree, J.W., and Isaac, J.T. (2002). A presynaptic kainate receptor is involved in regulating the dynamic properties of thalamocortical synapses during development. Neuron *34*, 635–646.

Knott, G.W., Quairiaux, C., Genoud, C., and Welker, E. (2002). Formation of dendritic spines with GABAergic synapses induced by whisker stimulation in adult mice. Neuron *34*, 265–273.

Knudsen, E.I. (2004). Sensitive periods in the development of the brain and behavior. J. Cogn. Neurosci. *16*, 1412–1425.

Lee, S.M., and Ebner, F.F. (1992). Induction of high frequency activity in the somatosensory thalamus of rats in vivo results in long-term potentiation of responses in SI cortex. Exp. Brain Res. *90*, 253–261.

Lefort, S., Tomm, C., Floyd Sarria, J.C., and Petersen, C.C. (2009). The excitatory neuronal network of the C2 barrel column in mouse primary somatosensory cortex. Neuron *61*, 301–316.

Lin, Y.J., and Koretsky, A.P. (1997). Manganese ion enhances T1-weighted MRI during brain activation: an approach to direct imaging of brain function. Magn. Reson. Med. *38*, 378–388.

Logothetis, N.K., Pauls, J., Augath, M., Trinath, T., and Oeltermann, A. (2001). Neurophysiological investigation of the basis of the fMRI signal. Nature *412*, 150–157.

Lu, H.C., Gonzalez, E., and Crair, M.C. (2001). Barrel cortex critical period plasticity is independent of changes in NMDA receptor subunit composition. Neuron *32*, 619–634.

Lu, H.C., She, W.C., Plas, D.T., Neumann, P.E., Janz, R., and Crair, M.C. (2003). Adenylyl cyclase I regulates AMPA receptor trafficking during mouse cortical 'barrel' map development. Nat. Neurosci. *6*, 939–947.

Maier, A., Wilke, M., Aura, C., Zhu, C., Ye, F.Q., and Leopold, D.A. (2008). Divergence of fMRI and neural signals in V1 during perceptual suppression in the awake monkey. Nat. Neurosci. *11*, 1193–1200.

Majewska, A.K., and Sur, M. (2006). Plasticity and specificity of cortical processing networks. Trends Neurosci. *29*, 323–329.

Malenka, R.C., and Bear, M.F. (2004). LTP and LTD: an embarrassment of riches. Neuron *44*, 5–21.

Mugler, J.P., 3rd, and Brookeman, J.R. (1990). Three-dimensional magnetization-prepared rapid gradient-echo imaging (3D MP RAGE). Magn. Reson. Med. *15*, 152–157.

Murayama, Y., Weber, B., Saleem, K.S., Augath, M., and Logothetis, N.K. (2006). Tracing neural circuits in vivo with Mn-enhanced MRI. Magn. Reson. Imaging *24*, 349–358.

Narita, K., Kawasaki, F., and Kita, H. (1990). Mn and Mg influxes through Ca channels of motor nerve terminals are prevented by verapamil in frogs. Brain Res. *510*, 289–295.

Ogawa, S., Lee, T.M., Stepnoski, R., Chen, W., Zhu, X.H., and Ugurbil, K. (2000). An approach to probe some neural systems interaction by functional MRI at neural time scale down to milliseconds. Proc. Natl. Acad. Sci. USA *97*, 11026–11031.

Paxinos, G., and Watson, C. (2007). The Rat Brain in Stereotaxic Coordinates, 6th Edition (Amsterdam: Elsevier).

Pautler, R.G., Silva, A.C., and Koretsky, A.P. (1998). In vivo neuronal tract tracing using manganese-enhanced magnetic resonance imaging. Magn. Reson. Med. *40*, 740–748.

Pelled, G., Bergman, H., Ben-Hur, T., and Goelman, G. (2007a). Manganese-enhanced MRI in a rat model of Parkinson's disease. J. Magn. Reson. Imaging *26*, 863–870.

Pelled, G., Chuang, K.H., Dodd, S.J., and Koretsky, A.P. (2007b). Functional MRI detection of bilateral cortical reorganization in the rodent brain following peripheral nerve deafferentation. Neuroimage *37*, 262–273.

Pelled, G., Bergstrom, D.A., Tierney, P.L., Conroy, R.S., Chuang, K.H., Yu, D., Leopold, D.A., Walters, J.R., and Koretsky, A.P. (2009). Ipsilateral cortical fMRI responses after peripheral nerve damage in rats reflect increased interneuron activity. Proc. Natl. Acad. Sci. USA *106*, 14114–14119.

Porter, J.T., Johnson, C.K., and Agmon, A. (2001). Diverse types of interneurons generate thalamus-evoked feedforward inhibition in the mouse barrel cortex. J. Neurosci. *21*, 2699–2710.

Raastad, M., Storm, J.F., and Andersen, P. (1992). Putative single quantum and single fibre excitatory postsynaptic currents show similar amplitude range and variability in rat hippocampal slices. Eur. J. Neurosci. *4*, 113–117.

Ramachandran, V.S. (2005). Plasticity and functional recovery in neurology. Clin. Med. *5*, 368–373.

Rees, G., Friston, K., and Koch, C. (2000). A direct quantitative relationship between the functional properties of human and macaque V5. Nat. Neurosci. *3*, 716–723.

Rema, V., Armstrong-James, M., Jenkinson, N., and Ebner, F.F. (2006). Short exposure to an enriched environment accelerates plasticity in the barrel cortex of adult rats. Neuroscience *140*, 659–672.

Sirotin, Y.B., and Das, A. (2009). Anticipatory haemodynamic signals in sensory cortex not predicted by local neuronal activity. Nature *457*, 475–479.

Stevens, C.F., and Wang, Y. (1995). Facilitation and depression at single central synapses. Neuron *14*, 795–802.

Sun, Q.Q., Huguenard, J.R., and Prince, D.A. (2006). Barrel cortex microcircuits: thalamocortical feedforward inhibition in spiny stellate cells is mediated by a small number of fast-spiking interneurons. J. Neurosci. *26*, 1219–1230.

Sun, Q.Q., Zhang, Z., Jiao, Y., Zhang, C., Szabó, G., and Erdelyi, F. (2009). Differential metabotropic glutamate receptor expression and modulation in two neocortical inhibitory networks. J. Neurophysiol. *101*, 2679–2692.

Tailby, C., Wright, L.L., Metha, A.B., and Calford, M.B. (2005). Activity-dependent maintenance and growth of dendrites in adult cortex. Proc. Natl. Acad. Sci. USA *102*, 4631–4636.

Tucciarone, J., Chuang, K.H., Dodd, S.J., Silva, A., Pelled, G., and Koretsky, A.P. (2009). Layer specific tracing of corticocortical and thalamocortical connectivity in the rodent using manganese enhanced MRI. Neuroimage *44*, 923–931.

Uğurbil, K., Toth, L., and Kim, D.S. (2003). How accurate is magnetic resonance imaging of brain function? Trends Neurosci. *26*, 108–114.

Van der Linden, A., Verhoye, M., Van Meir, V., Tindemans, I., Eens, M., Absil, P., and Balthazart, J. (2002). In vivo manganese-enhanced magnetic resonance imaging reveals connections and functional properties of the songbird vocal control system. Neuroscience *112*, 467–474.

Van der Linden, A., Van Meir, V., Boumans, T., Poirier, C., and Balthazart, J. (2009). MRI in small brains displaying extensive plasticity. Trends Neurosci. *32*, 257–266.

Van der Loos, H., and Woolsey, T.A. (1973). Somatosensory cortex: structural alterations following early injury to sense organs. Science *179*, 395–398.

van der Zijden, J.P., Bouts, M.J., Wu, O., Roeling, T.A., Bleys, R.L., van der Toorn, A., and Dijkhuizen, R.M. (2008). Manganese-enhanced MRI of brain plasticity in relation to functional recovery after experimental stroke. J. Cereb. Blood Flow Metab. *28*, 832–840.

van Meer, M.P., van der Marel, K., Otte, W.M., Berkelbach van der Sprenkel, J.W., and Dijkhuizen, R.M. (2010). Correspondence between altered functional and structural connectivity in the contralesional sensorimotor cortex after unilateral stroke in rats: a combined resting-state functional MRI and manganese-enhanced MRI study. J. Cereb. Blood Flow Metab. *30*, 1707–1711.

Wall, J.T., Xu, J., and Wang, X. (2002). Human brain plasticity: an emerging view of the multiple substrates and mechanisms that cause cortical changes and related sensory dysfunctions after injuries of sensory inputs from the body. Brain Res. Brain Res. Rev. *39*, 181–215.

Wallace, H., and Fox, K. (1999). The effect of vibrissa deprivation pattern on the form of plasticity induced in rat barrel cortex. Somatosens. Mot. Res. *16*, 122–138.

Wimmer, V.C., Broser, P.J., Kuner, T., and Bruno, R.M. (2010). Experience-induced plasticity of thalamocortical axons in both juveniles and adults. J. Comp. Neurol. *518*, 4629–4648.

Woolsey, T.A., and Van der Loos, H. (1970). The structural organization of layer IV in the somatosensory region (SI) of mouse cerebral cortex. The description of a cortical field composed of discrete cytoarchitectonic units. Brain Res. *17*, 205–242.

Yu, X., Wadghiri, Y.Z., Sanes, D.H., and Turnbull, D.H. (2005). In vivo auditory brain mapping in mice with Mn-enhanced MRI. Nat. Neurosci. *8*, 961–968.

Yu, X., Sanes, D.H., Aristizabal, O., Wadghiri, Y.Z., and Turnbull, D.H. (2007). Large-scale reorganization of the tonotopic map in mouse auditory midbrain revealed by MRI. Proc. Natl. Acad. Sci. USA *104*, 12193–12198.

Yu, X., Zou, J., Babb, J.S., Johnson, G., Sanes, D.H., and Turnbull, D.H. (2008). Statistical mapping of sound-evoked activity in the mouse auditory midbrain using Mn-enhanced MRI. Neuroimage *39*, 223–230.

Yu, X., Wang, S., Chen, D.Y., Dodd, S., Goloshevsky, A., and Koretsky, A.P. (2010). 3D mapping of somatotopic reorganization with small animal functional MRI. Neuroimage *49*, 1667–1676.